LASER INTERFEROMETER GRAVITATIONAL WAVE OBSERVATORY
- LIGO -
CALIFORNIA INSTITUTE OF TECHNOLOGY
MASSACHUSETTS INSTITUTE OF TECHNOLOGY

Document Type	LIGO-T050059-01-D	2005/09/01

Calibration of the LIGO detectors for S3

Gabriela González, Mike Landry, Brian O'Reilly, Xavier Siemens

Distribution of this draft:

LIGO Scientific Collaboration

Processed with LaTeX on 2005/09/01

Abstract

We describe the methods used to calibrate the LIGO interferometer responses for the S3 run, as well as results and an error analysis.

1 Introduction

The third LIGO Scientific Run, S3, consisted of data taken with the three LIGO detectors, from Friday October 31, 2003 through Friday January 9, 2004. This document is intended as a summary of the techniques used to calibrate the response of the interferometers and an estimate of associated uncertainties. Those readers wishing to skip the details can find a convenient summary in Table 9.

As in previous runs[1, 2], we consider the response of the interferometer to an external strain disturbance (e.g. a gravitational wave) to be that of a single degree of freedom feedback loop on the difference of arm lengths, characterized by a loop gain function $G(f)$ (see Figure 1). This loop can be parameterized by three functions: a "Sensing" function $C(f)$ which describes the free response of the error signal IFO:LSC-AS_Q to the strain disturbance, in units of ASQcounts/strain; a "Digital Filter" function $D(f)$, or the response function of the control signal IFO:LSC-DARM_CTRL to the error signal IFO:LSC_AS_Q, in units of DARMcounts/ASQcounts; and an "Actuation" function $A(f)$ which describes the free response of the strain produced by the control signal, in units of strain/DARMcounts.

These functions are related by

$$G(f) = C(f)A(f)D(f). \tag{1}$$

The actuation function, $A(f)$, is essentially the suspension pendulum transfer function, modified by the actuation electronics chain (with analog and digital filters that compensate each other). We assume that the function $A(f)$ does not change during the run.

The sensing function $C(f)$ is essentially a cavity pole function, scaled by the optical gain in the detector. Since the optical gain depends on the fluctuating alignment, the sensing function is a function of time and frequency, which we assume is of the form $C(t, f) = \alpha(t)C_0(f)$, where $C_0(f)$ is the sensing function at some reference time t_0.

The digital filter function $D(f)$ is in general a complicated function of frequency with the appropriate filters for producing a conditionally stable feedback loop with a unity gain frequency around 150 Hz. In order to keep the feedback loop gain stable, a digital coefficient in the loop is scaled with measurements of carrier power in the arms, and sideband power in the recycling cavity. Therefore, the function $D(f)$ is also dependent on time in the form $D(t, f) = \beta(t)D_0(f)$. The loop gain is then $G(t, f) = \alpha(t)\beta(t)G_0(f)$, with $G_0(f) = C_0(f)D_0(f)A(f)$. We assume the functions $\alpha(t), \beta(t)$ vary with time, but with spectral content only at frequencies below 40 Hz, below the gravitational wave band.

The Fourier transform of the strain sensitivity of the interferometer at a time t, $h(f, t)$ is related to the Fourier transform $ASQ(t, f)$ of the signal IFO:LSC-AS_Q by:

$$h(f, t) = R(t, f)AS\_Q(t, f) \tag{2}$$

with

$$R(t, f) = \frac{1 + G(t, f)}{C(t, f)} = \frac{1 + \alpha(t)\beta(t)G_0(f)}{\alpha(t)C_0(f)}. \tag{3}$$
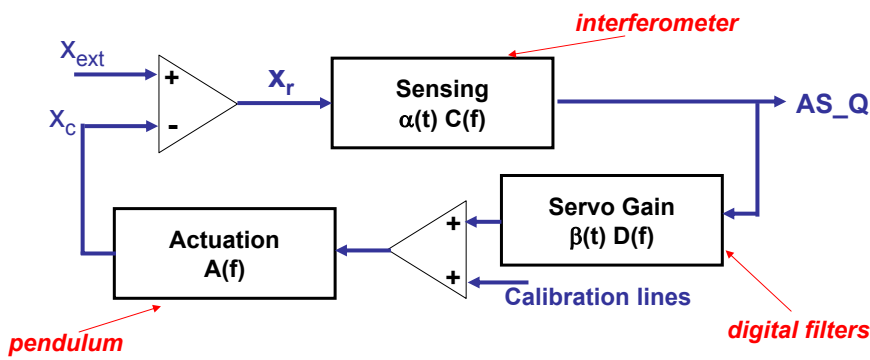
Figure 1: Block diagram of the interferometer

We call $R(t, f)$ the response function for the interferometer. In practice we can obtain direct measurements of $G_0(f), A(f), \alpha(t)$ and $\beta(t)$, but not of the sensing function $C_0(f)$. We use Equation 1 to find $C_0(f)$ from our measurements of $G_0(f)$, $A(f)$ and $D_0(f)$.

The calibration products posted in the Calibration web page:

`http://blue.ligo-wa.caltech.edu/engrun/Calib_Home/`

are, for each detector:

- a text file with a lookup table for the reference functions as a function of frequency ($C_0(f)$, $G_0(f)$, $R_0(f)$)

- a frame file containing the reference functions R_0, C_0,

- the actuation function $A(f)$,

- a text file with the time history of the calibration coefficients $\alpha(t)$, $\beta(t)$, and

- a frame file with the calibration coefficients $\alpha(t)$, $\beta(t)$.

The reference functions G_0, C_0, A, and R_0 for each detector are created with a Matlab function "LSCmodel.m", first written for S1 and S2 by Rana Adhikari, that reads in parameters for the detector model and a frequency vector, and creates complex output vectors for the open loop gain, sensing and actuation functions, and the response function. The parameters used in the detector model are mostly taken from measurements described later, with a few free parameters that are used to fit the model open loop gain to a measurements. The matlab models and parameter files are posted in the calibration web page.

The coefficients α, β are measured from complex ratios of demodulated time series of the signals IFO:LSC-AS_Q, IFO:LSC-DARM_CTRL, and IFO:LSC-DARM_CTRL_EXC. There are three calibration lines injected, and we test for consistency of the results from each line, which is a test of the assumption that $G(t, f)$ is a real scalar coefficient ($\alpha(t)\beta(t)$) times a constant function of frequency $G_0(f)$.

In the sections that follow, we describe the procedures used to create the calibration products, and the estimated errors associated with the measurements and models used.

1.1 The Actuation Function $A(f)$

The actuation chain, from a signal in IFO:LSC-DARM_CTRL to a change in the differential arm length made through the push in the four magnets in each end test mass, is made from the following components:

- LSC output matrix coefficients, splitting the signal into inputs to the ETMX and ETMY digital suspension controllers;

- digital filters in the LSC filter bank, in each of the ETMX, ETMY digital suspension controllers;

- coil gain coefficients in the LSC-POS matrix;

- coil digital filters in the (LL, LR, UR,UL)POS filter banks (including force-to-pitch filters)

- coil digital filters in the (LL, LR, UR,UL)COIL filter banks (including the "AntiDewhite" filters);

- anti-imaging filter;

- digital to analog module;

- coil analog filters (including dewhitening filters);

- analog coil driver "snubber" filters;

- coil-magnet actuation gains;

- suspended mirror transfer function (pendulum).

- for H1 and H2 only, a residual transfer function is included to account for insufficient digital compensation of the dewhitening filters (the residual is described below)

There is also a time delay due to the light travel time in the arm cavities, plus possibly time delays in the digital and analog systems, which only affects the phase of the actuation function (and of the open loop gain). The time delay is one of the parameters we use to fit our measured open loop gain to the model.

The digital suspension filters "AntiDewhite" for each coil compensate the frequency response of the analog dewhitening filters, to produce a unity transfer function. Also, the "force to pitch" filters are tuned to produce a single pendulum response for a piston motion of the mass (rather than a coupled pendulum-pitch response). The pendulums for both test masses have the same frequency, and although they don't necessarily have the same quality factor (appropriate for the damping in each), the damping function does not affect the pendulum transfer function at frequencies in the gravitational wave band (40 Hz-2 kHz). Thus, although there are many components to this function, in principle it all boils down to a simple pendulum transfer function, with a scale factor that we call the "DC gain", setting the value of the actuation at zero frequency.

In Matlab, we model the actuation function in "LSCmodel.m" (in the Laplace domain) as a product of the following functions: a pendulum function `lscpend`, an anti-imaging filter `ai`; a time delay `tdelay`; a snubber filter `snub`; a digital-to-analog filter `d2a`; and a function `(hd1+hd2)/2`, where `hdn` is the digital filter corresponding to each mass.

The poles and zeros of the as-built analog dewhitening filters are slightly different than those of the designed filters. Thus, if the digital compensation of the dewhitening filters is done using the designed parameters, there will be a frequency dependence in the actuation function due to the imperfect compensation. In L1, the transfer function for each one of the eight dewhitening filters (one for each coil in ETMx and ETMY) was carefully measured and properly compensated with digital filters (see entry by Brian O'Reilly in the LLO elog on Oct 4, 2003). The differences between design and measurements were up to 5% in magnitude and 5 degrees in phase; the residuals after the fit were better than 1% in magnitude and 1 degree in phase. In H1, the digital filters had the poles and zeros of the design, rather than the actual as-built ones. This was taken into account measuring the transfer function of the filters; modeling them with a single transfer function; calculating the product of the digital filters and a model for the dewhitening filters; and including the modeled residual in the model for the actuation function.

- Pendulum function:

  ```
  darm.DCcal * tf(wp^2, [1 wp/Qp wp^2]);
  ```

- Pendulum DC calibration

  ```
  darm.DCcal = darm.ETMYcal * darm.darm2etmy -...
          darm.ETMXcal * darm.darm2etmx;
  ```

- Anti-imaging filter:

  ```
  [z,p,k] = ellip(4,4,60,2*pi*7570,'s');
  misc.ai = zpk(z,p,k*10^(4/20)) * zpk([],-2*pi*13e3,2*pi*13e3);
  ```

- Time delay:

  ```
  [num,den] = pade(lsc.tdelay,4);
  tdelay = tf(num,den);
  ```

- Coil driver snubber filter:

  See LLO elog entry by Brian O'Reilly on Feb 8, 2003.

- Digital to analog filter (as a function of frequency):

$$\text{d2a}(f) = \frac{sin(2\pi f/f_s)}{2\pi f/f_s} e^{-i\pi f/f_s},$$

  with f_s=16384 Hz being the sampling frequency.

- Digital suspension filters are read from the suspension digital filter files IFOSUS_ETM#.txt used during the science run, selecting the filters that were on at the time.

Table 1 shows the input parameters in the Matlab files "IFOparameters.m" that correspond to the actuation function.

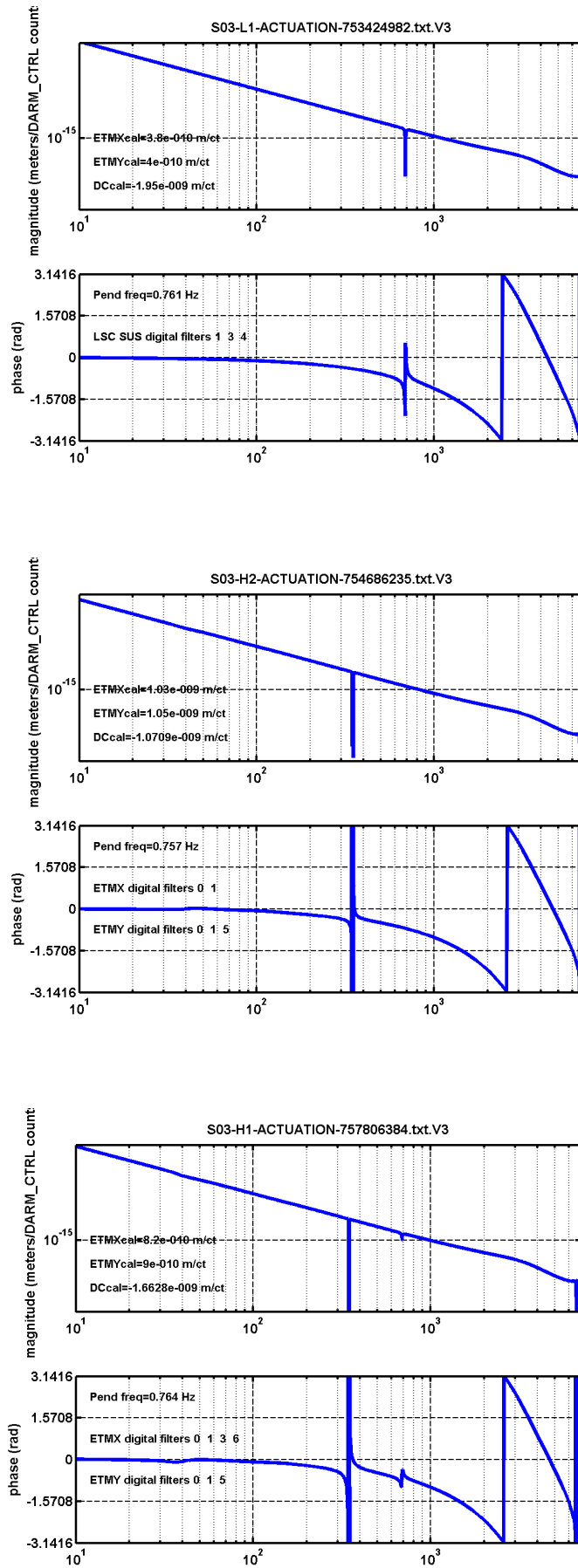Figure 1.1 shows the actuation functions for all three detectors.

S03-L1-ACTUATION-753424982.txt.V3

ETMXcal=3.8e-010 m/ct

ETMYcal=4e-010 m/ct

DCcal=-1.95e-009 m/ct

Pend freq=0.761 Hz

LSC SUS digital filters 1 3 4

S03-H2-ACTUATION-754686235.txt.V3

ETMXcal=1.03e-009 m/ct

ETMYcal=1.05e-009 m/ct

DCcal=-1.0709e-009 m/ct

Pend freq=0.757 Hz

ETMX digital filters 0 1

ETMY digital filters 0 1 5

S03-H1-ACTUATION-757806384.txt.V3

ETMXcal=8.2e-010 m/ct

ETMYcal=9e-010 m/ct

DCcal=-1.6628e-009 m/ct

Pend freq=0.764 Hz

ETMX digital filters 0 1 3 6

ETMY digital filters 0 1 5

Figure 2: Actuation functions for the LIGO detectors during S3.

Parameter	L1	H1	H2
Arm length (m)	3995.1	3995.064	2009.12
Pendulum wp	$2\pi 0.761$ Hz	$2\pi 0.764$ Hz	$2\pi 0.757$ Hz
Pendulum Qp	10	10	10
Output matrix coefficients darm2etmx, darm2etmy	2.50,-2.50	1.04, -0.90	0.53, -0.50
ETM DC calibrations ETMX, ETMY (nm/ct)	0.38, 0.40	0.82, 0.90	1.03, 1.05
DARM DC cal (nm/ct)	1.95	1.66	1.07
Time delay (μs)	165	147.5	148.94
ETMX SUS Filters	#1(Violin2) #3(Drumhead) #4(Ellip6648)	#0(TMNotch) #1(violinSB) #3(TM6622) #6(violin2)	#0(TMnotch) #1(violinSB)
ETMY SUS Filters	FM1(Violin2) #3(Drumhead) #4(Butterfly)	#0(TMnotch) #1(violinSB) #5(TM6622)	#0(TMnotch) #1(violinSB)

Table 1: Parameters used in the model for the actuation function.

1.2 Error estimates: DC calibration

We can describe the error associated with the actuation function as an overall gain error, due to the DC calibration, and a frequency-dependent error, arising from imperfect modeling. Since we do not have a direct measurement of the frequency dependence of the actuation function (other than the measurement of the open loop gain, containing the actuation function), we will assume a frequency-independent error equal to the error in the DC calibration. This error depends strongly on the measurement procedure, described in the following paragraphs.

1.2.1 LLO measurements

As described in [2], the response of the end test masses (ETMs) to an excitation in IFO:LSC_DARM_CTRL can be measured in several different ways, to obtain values and error for the model parameters darm.ETMxcal and darm.ETMYcal.

At LLO, the ITMs were calibrated with a simple Michelson, and then the ETMs were calibrated against the ITMs with single arm measurements. These measurements have the advantage of being done in the gravitational wave band, but on the other hand they are sensitive to mismatches in digital and analog filters in the sensing and actuation chain that imperfectly compensate each other. In the simple Michelson interferometer, the response of ASQ to ITM excitation should show a pendulum response; in the single arm measurements, the ratio of the response of ASI to ITM and of ASI to ETMX should be frequency independent. Two sets of measurements were done, on November 8 2003 and on January 9 2004. In both cases, the ASQ response to ITM excitation was consistent with a pendulum response for frequencies above 200 Hz. (At lower frequencies, the measurement was affected by non-negligible loop gain.) Results from both measurement dates were indistinguishable within the measurement error. The results obtained for the DC response of

an ITM pendulum with frequency 0.76 Hz were

$$dx/d(ITMX\_EXC) = (0.420 \pm 0.010)\text{nm/ct, and}$$
$$dy/d(ITMY\_EXC) = (0.435 \pm 0.010)\text{nm/ct.}$$

The single arm measurements, done to calibrate the ETMs against the ITMs, showed a significantly non-flat ratio of (dASI/dETM*_EXC) / (dASI/dITM*_EXC), with a 10% step between 200 and 500 Hz. This is most likely caused by uncompensated "acquire" filters in the ETMs (since the measurement could not be done in the "run" mode, for which the filters were well measured and compensated). The ETM/ITM ratios measured on both dates had the same features, but the mean values in each case were different by 5-10%.

The standard deviation of the ETM/ITM ratio function in the frequency range where the ITM measurements were valid is only 5%, but given the uncertainty in the measurement, we adopt a conservative estimate of 10% for the error in the ETM DC calibration for the values used in the model. Thus, the values adopted for the DC response of an ETM pendulum with frequency 0.76 Hz were

$$dx/d(ETMX\_EXC) = (0.38 \pm 0.04)\text{nm/ct, and}$$
$$dy/d(ETMY\_EXC) = (0.40 \pm 0.04)\text{nm/ct.}$$

Fig.1.2.1 show the measurements taken on both dates.

1.2.2 Hanford measurements

A DC calibration method with smaller statistical uncertainty is *sign-toggling* [3]. The calibration is not made in the gravity-wave band (as in the case of the measurements at LLO described above), but can achieve high precision through repeated trials. A simple Michelson interferometer is locked on a (bright) fringe, and the sign of the feedback control loop toggled, so that the controlled mass then moves through $\lambda/4$ to a neighbouring (dark) fringe. The control signal required to lock this configuration jumps discretely once the sign is flipped, and the size of the jump reveals a DC calibration in nm/count. This procedure yields a precision ($\sim$1%) DC calibration for an input test mass (ITM). However, what is required for a calibration of the DARM loop is a DC calibration of the end test masses (ETMs), so the ITM calibration must be transferred by using a Fabry-Perot cavity in a single arm of the detector, and injecting sinusoidal disturbances into the arm (on both input and end test masses, again, as noted above). The transfer process adds uncertainty and the ETM DC calibration, which can have a resultant error of 6% [2]. If the ETM is calibrated directly, the uncertainty associated with the transfer is eliminated.

For S3, an asymmetric Michelson configuration was locked, in which an ITM and an opposing ETM were aligned (see Figure 4, in which an ITMY and an ETMX are aligned, while masses ITMX and ETMY are misaligned). The asymmetric Michelson was locked by feeding back to the ETM; the sign of the control signal was flipped and the DC readout at the antisymmetric port changed. The result is a $\sim$1% calibration of the H2 ETMs: statistical uncertainty on the H2 ETMX DC calibration was 1%, while H2 ETMY was 2%. This method was also employed on the H1 ETMX, but the data were noisier (smaller contrast defect with the longer arm), so that the calibration error was larger: 5% for H1 ETMX. In summary, the improved asymmetric Michelson DC calibration was performed for the H2 instrument (both X and Y ETMs), and the H1 X arm. The DC calibration for the Y-arm was obtained through a PZT fine actuator measurement, as described
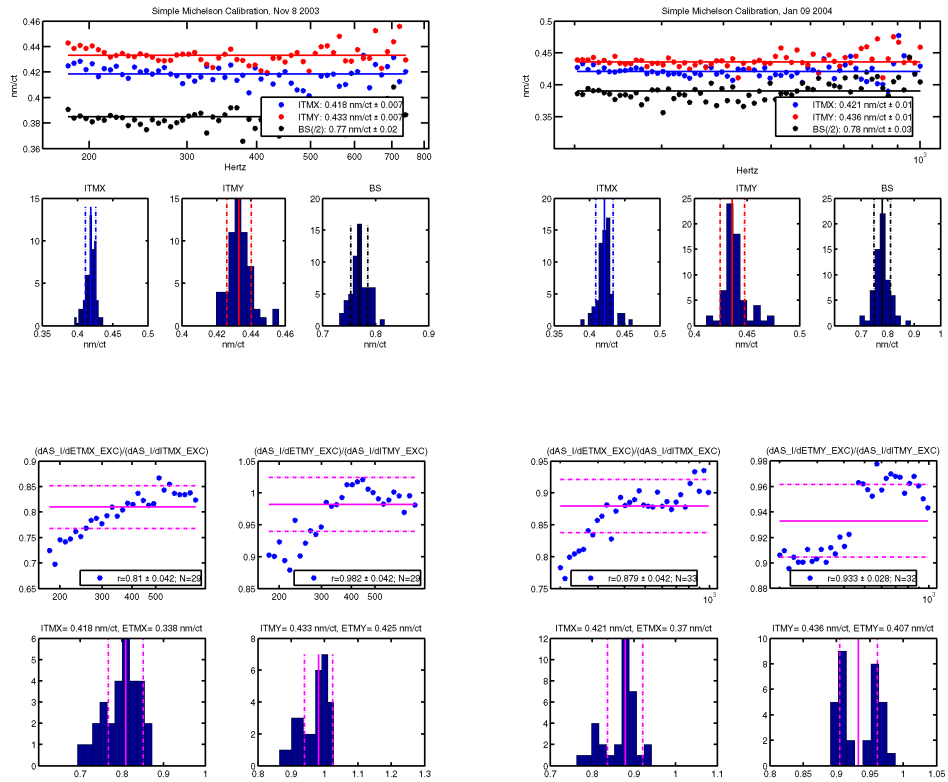
Figure 3: DC calibration measurements measurements with a simple Michelson (top row) and single arms (bottom row). The measurements in the left column were taken on November 8, 2003; the ones in the the right column were taken on January 9, 2004.
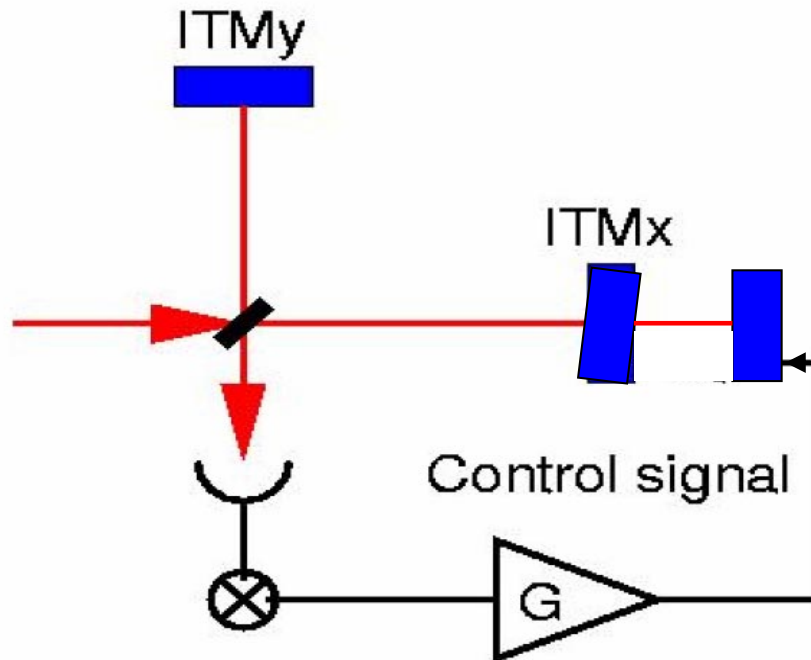
Figure 4: Schematic of an example asymmetric Michelson configuration. The Michelson is locked via feedback to the ETMX. Light passes twice through the partially-transmitting ITMX, which is misaligned at some arbitrary angle. DC readout at the antisymmetric port consists predominantly of the direct reflection off of the ITMY (bright) with a small component of light from the opposing ETMX added (brighter) or subtracted (darker).

in [2], and made post-S3 at LHO, with an uncertainty of 6%. DC calibration errors are summarized below.

1.2.3 DC calibration errors: summary

The DC actuation function measurements and its errors are summarized in Table 2.

IFO	ETMX (nm/ct)	ETMY (nm/ct)	DC cal (nm/ct)
L1	0.38 ± 0.04	0.40 ± 0.04	1.95 ± 0.30
H1	0.82 ± 0.05	0.90 ± 0.05	1.66 ± 0.14
H2	1.03 ± 0.01	1.05 ± 0.02	1.07 ± 0.02

Table 2: Summary of measurements of the DC values of the actuation functions for all three interferometers.

1.3 The sign of the calibration

The respective IFO signs of the calibration [2] were the same as in S2, since there were no hardware or software changes in the DARM loop that changed the sign in any detector. This was validated with drives to the fine actuators in the vacuum chambers at the mid station (for H2), and with hardware injections performed by the stochastic group (for H1/L1 software/hardware injections). Sensing signs were also re-measured on H1 and H2. The actuation sign is thus negative for all three detectors; the sensing sign is positive for the LHO detectors and negative for L1; the input matrix sign is negative for the LHO detectors, and positive for L1. All three IFOs had negative DARM gains for S3.

2 The Digital Filter function $D(f)$

This part of the loop is modeled using the DARM filters in the actual filter files loaded in the LSC during S3, "IFOLSC.txt". The only parameters in the parameter file used in the matlab model, other than the filters chosen from the filter file, are the value of the input matrix and of the LSC gain at the time of the reference measurement. The value of the input matrix is obtained averaging it for 10 minutes around the reference time. Table 3 summarizes the filters used in each detector and the digital function parameters. The only error associated with the digital function is the error in the estimate for the input matrix, which is averaged near the reference time, when the open loop gain is measured. The distribution of the measured values in L1 during 500 seconds around the reference time, shown in Fig.2 is reasonably Gaussian, with a 8% width. The error assigned to the mean of the distribution, which used 500 points, is 0.3%; however, we estimate the error as the one scaled to minute trends, which is what we use for calibration coefficients, or 2%.

3 Sensing function C(f)

The sensing function C(f) is the transfer function between a differential strain and the digital signal in Xn:LSC-AS_Q, in the absence of a feedback loop, measured in counts . The frequency dependence of the optical transfer function is just a real pole due to the arm cavities (LIGO-T970084-00).

Parameter	L1	H1	H2
LSC DARM Filters	#0$(0^2 : 30^2)$	#0 $(0^2 : 20^2)$	#0 (0,0:30,30)
	#1$(1k^2 : 10, 90)$	#1 $(1k^2 : 10, 100)$	#1 (2K:10,100)
	#2(2kBW)	#2 (4kBW)	#2 (2kBW)
	#3(Boo)	#3 (MadBoost)	#3 (MadBoost)
		#4 (lead150)	
		#7 (RG12,17.6)	
Reference GPS time	753424982	757806384	754686235
Input matrix	+0.00128	-0.00065125	-0.00521
DARM gain	-1.7	-2.2	-0.545

Table 3: Parameters used in the model for the digital filter function

Figure 5: L1 Input matrix coefficient during the reference time.

We assume the frequency response of the photodiode and of the demodulator board is frequency-independent. In L1, there was an RC low pass filter after the mixer, modelled with a single real pole at 16 kHz. The anti-aliasing filter is modelled as an elliptic filter and a pole at twice the sampling frequency. The analog whitening filter is compensated by a digital anti-whitening filter before the signal is written to disk as AS_Q, so we assume there is no frequency-dependent transfer function.

The overall gain, as well as the frequency dependence of the sensing function, are not directly measurable; we resort instead to the measurement of the open loop function $G(f) = D(f)A(f)C(f)$, described in the following section. We check the consistency of the frequency dependence of $G(f)$ with the one assumed in the mdoel; we adjust an overall gain in $G(f)$ to match the measurement, and then obtain the gain for $C(f)$ from the ratio $G(f)/(A(f)D(f))$.

The arm cavity poles in L1 were measured and elogged by Andi Gretarsson on July 20, 2003. The arm cavity poles for H1 and H2 were measured and elogged by Joe Betzwiezer on February 20 2004. In all cases, the measurement error was 1%, about the same as the diffference between the values for the different arms (in the DARM matlab model, we used a single cavity pole). The measured values of the cavity poles, the values used in the model, and the measurement errors (not

including possible systematic errors) are shown in Table 4.

Follow up measurements suggest that the measurements of cavity poles may be subject to a systematic error of as much as 4 Hz. We show in Fig 3 the differences in magnitude and phase that can result from such a difference in the pole cavity, for H1/L1 (where the pole is at 83 Hz) and H2 (where the pole is at 160 Hz). The difference in magnitude and phase is frequency dependent, with the maximum error in magnitude of 5% for L1, H1 and 2.5% in H2 (at frequencies significantly higher than the pole), and in phase of 1.5deg in L1, H1 and 0.75 deg in H2, at the pole frequencies.

In principle, since we do not have a direct measurement of the sensing function, the consequence of using a wrong cavity pole is a discrepancy in the matching of the model and measurement of the open loop gain function $G(f)$. As we will show, although there is no evidence of a discrepancy between model and measurement that can be simply explained by a difference in the cavity pole used, the measured discrepancies and the measurement errors cannot rule out a systematic error in the cavity pole of 4 Hz. The discrepancies between model and measurement of the phase of G(f) are strongly affected by the time delay chosen for the actuation function, so again we cannot rule out a systematic error in the cavity pole. The error in magnitude of the sensing function will be accounted in the response function (expressed in terms of A, D and G) by the error in G. The error in phase of C, however, will be accounted by an error in A due to the time delay, which we estimate at 1.5 deg for H1, L1 and 0.75deg in H2.

Detector	X-arm	Y-arm	DARM Model
L1	83.6 Hz	81.6 Hz	82.6 Hz $\pm$ 1.2 Hz
H1	84.1 Hz	82.5 Hz	83.3 Hz $\pm$ 1.2 Hz
H2	160 Hz	157 Hz	160 Hz $\pm$ 2 Hz

Table 4: Measured cavity poles, and value used in the calibration model for the DARM loop.

We show in Fig.3 the sensing functions resulting from our model, for all three detectors.

4   The Open Loop Gain $G(f)$

The open loop function is measured by injecting a swept sine excitation into the loop and the IFO:LSC-DARM_EXC point, and recording the ratio IFO:LSC-DARM_IN2/IFO:LSC-DARM_IN1. The measurement is taken with the instrument set for normal data taking (but not in Science mode), at the times chosen as reference times, indicated in Table 3.

The Matlab model produces an open loop gain function $G(f) = A(f)D(f)C(f)$, with the actuation functions and digital functions described in the previous sections. The modeled open loop gain function is then compared to the measurement, and the unity gain frequency and the time delay are adjusted to match the measurement in amplitude and phase, respectively. The adjustment of the unity gain frequency is an overall gain factor; while the adjustment of the time delay in the actuation function changes the phase, but not the magnitude, of the model for $G(f)$. The residual difference in magnitude and phase is taken as the error in the model for the open loop gain function $G(f)$. The unity gain frequencies and phase margins of the measured loop gains are shown in Table5.

The comparisons between model and measurements are shown in Fig 8. Although the differences show a frequency dependence, we simplify the error analysis using a frequency independent
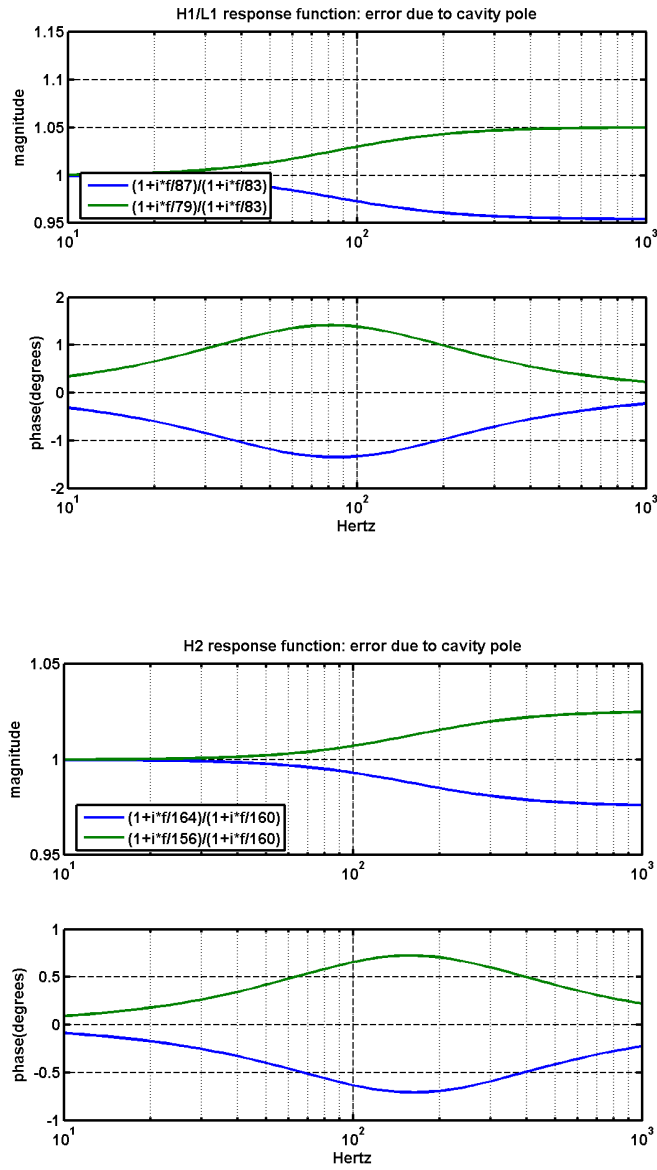
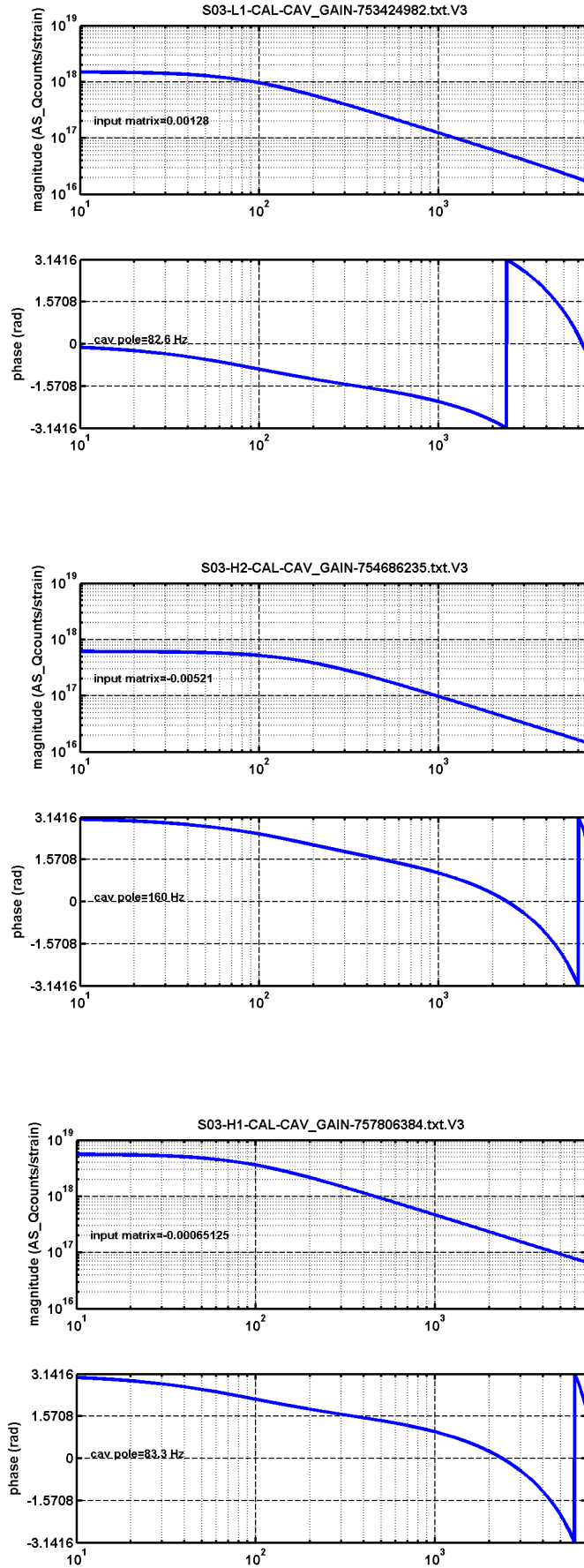Figure 6: Ratios of sensing function using different cavity poles

Figure 7: Sensing functions for the LIGO detectors during S3.

IFO	GPS	ugf, phase margin	meast/model(magnitude)	meast/model (phase)
L1	753424982	170 Hz, 34 deg	(0%, 5%)= 5%	(0, 1deg) =1 deg
H1	757806384	166 Hz, 50 deg	(2%, 4%) = 4%	(0, 2deg)=2 deg
H2	754686235	140 Hz, 39 deg	(8%, 6%) = 10%	(1.5deg, 1.4deg) = 2 deg

Table 5: Unity gain frequency and phase margin for DARM loop; errors in magnitude ($\Delta|G_{meas}(f)/G_{model}(f)|$) and phase ($\Delta\Theta(G_{meas}(f)/G_{model}(f))$) for G(f), between 60 Hz and 2 kHz. The error estimates in brackets are the estimates for systematic and random (measurement) error.

error for $G(f)$ in magnitude and phase, as indicated in Table 5. The error is the sum, in quadrature, of the error in the mean (if different from unity) and the standard deviation of the measurements.
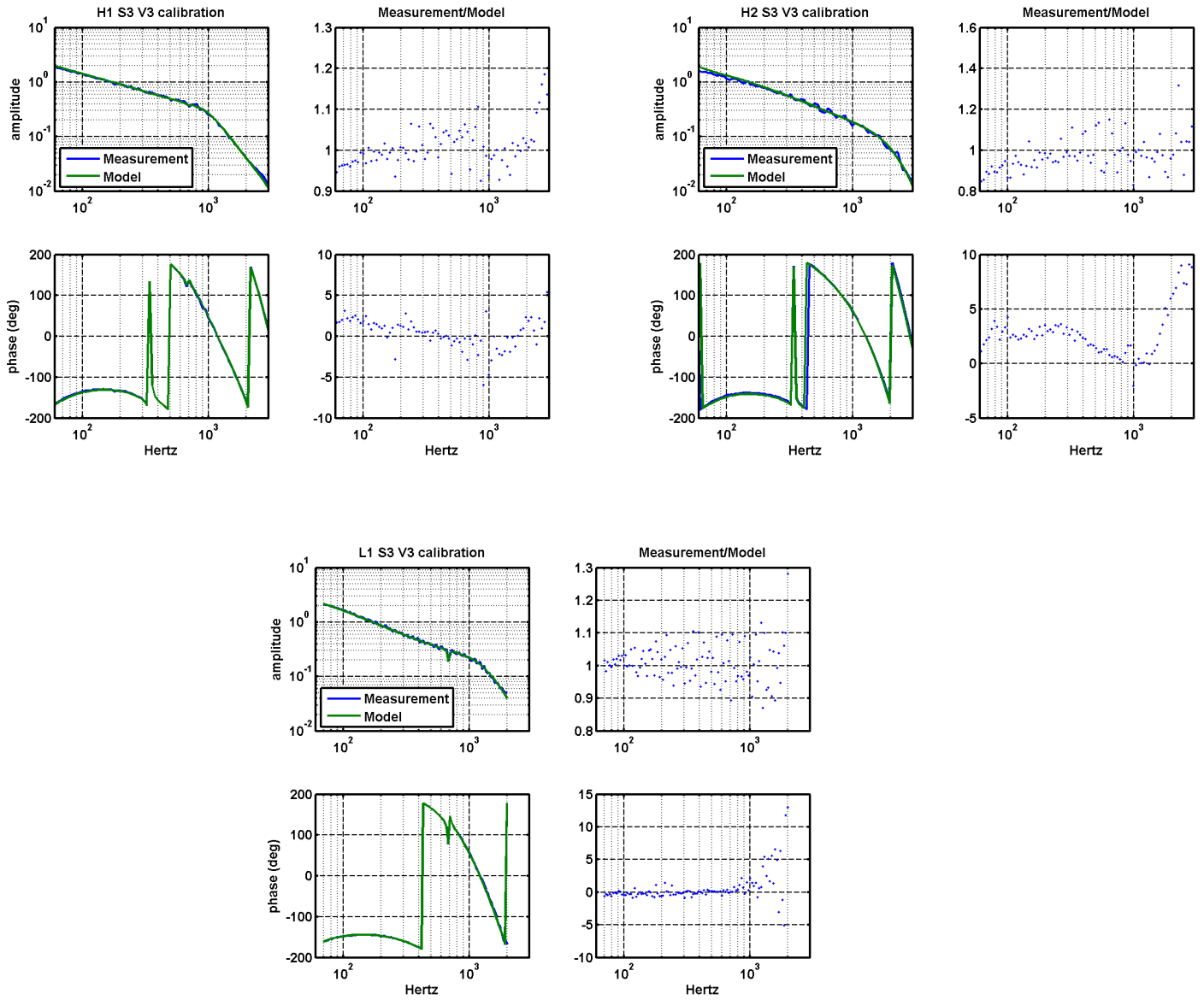
Figure 8: Comparison of model and measurement for open loop gain function G(f), for each detector

5 Calibration Coefficients α, β

In previous runs, the calibration coefficient β was fixed within a science segment, determined by the fixed digital values of the input matrix converting AS_Q into the error signal DARM_ERR, and the loop gain L1:LSC-DARM_GAIN. There were a few discrete values during the run, when one or both of these coefficients were changed. During the commissioning previous to S3, an algorithm was developed [4] where the input matrix coefficient was "dynamical", calculated by the front end computer code from transmitted arm powers and IFO:LSC-LA_SPOB, a signal proportional to the sideband power. The goal of this code was to compensate for changes in the optical gain in the detector (namely, the coefficient α) with an equal and opposite change in the digital gain (the coefficient β), to keep the DARM loop gain (the product $\alpha\beta$) constant. The effect is shown in the narrower distribution of $\alpha\beta$ in S3 than of each of α, β, as shown in Figs. 14, 16, 18.

In previous science runs, and in versions V1 and V2 of the S3 calibration, we calculated the calibration coefficients from the results produced by SenseMon, measuring the amplitude of the calibration line in AS_Q. The line amplitude was measured from the power spectrum of ASQ, averaged every minute.

For the final version V3 of the S3 calibration, the calibration coefficients were calculated digitally heterodyning the error and control signals AS_Q and DARM_CTRL, and excitation signal DARM_CTRL_EXC, with a sinusoid at the frequency used to produce to the calibration excitation. As can be deduced from Fig 1, if we have complex time series for the calibration line in ASQ, DARM and EXC, we can calculate the calibration coefficients using the following formulas:

$$
\begin{aligned}
\alpha\beta &= -\frac{1}{g_0}\frac{DARM - EXC}{DARM} \\
\alpha &= -\frac{d_0}{g_0}\frac{ASQ}{DARM} \\
\beta &= \frac{1}{d_0}\frac{DARM - EXC}{ASQ}
\end{aligned}
\tag{4}
$$

where g_0 is the reference open loop gain function evaluated at the calibration frequency: $g_0 = G_0(f_{cal})$, and d_0 is the reference digital filter function evaluated at the calibration frequency: $d_0 = D_0(f_{cal})$. In the absence of any input or noise other than the injected calibration line, the resulting coefficients are real. At the reference time, they are identically equal to one. In the presence of noise in ASQ (from any source), with spectral amplitude $S(f)$ around the calibration line, the calculated coefficients α and $\alpha\beta$ will have an imaginary part. If $S(f) = S_0$ is white Gaussian noise, the imaginary component will be a random variable, with zero mean, and standard deviation equal to $\sqrt{1.5 S_0 f_s}$, where f_s is the sampling frequency for the time series. The β coefficient should be real even in the presence of noise (since DARM and ASQ are related by a digital filter).

We calculate the coefficients taking the real part of the time series obtained from the formulas shown above. The imaginary part is used to measure the error in the real part. The mean of the imaginary part, if not zero, represents an error in the phase of the coefficients d_0 and/or g_0, which are obtained from the reference models described in previous sections. The magnitude of the coefficients d_0 and g_0 determines the value of the calibration coefficients at the reference time, which should be unity. Apart from the data in ASQ, DARM and EXC, the value of d_0 determines the magnitude and phase of β, and the value of g_0 determines the magnitude and phase of $\alpha\beta$.
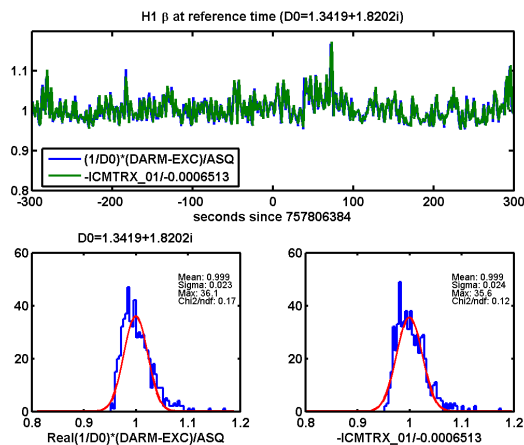
Figure 9: Coefficient β during reference time, calculated from demodulated lines and from input matrix values.

Of course, the value of β can also be obtained from the digital coefficient IFO:LSC-ICMTRX_01 which is written to frames; however, it is easier to work with α, β produced in the same format by the same script, than to use data from frames for β and from the lalapps code for α. However, we use the data in frames to validate the production of β from the code. We show in Fig5 the comparison of the time series and distributions for β calculated both ways.

We use Xavier Siemen's lalapps code "ComputeFactors.c" to compute the coefficients at the reference time, during hardware injection times, and in science segments. The code can be found in the calibration folder of the CVS repository:

http://www.lsc-group.phys.uwm.edu/cgi-bin/cvs/viewcvs.cgi/lalapps/src/calibration/

The arguments to the code are:

```
-f      FLOAT    Calibration line frequency in Hz.
-t      FLOAT    Time interval to calculate factors
                         in seconds (>0.0005).
-i      FLOAT    Real part of the open loop gain at the
                         calibration line frequency.
-j      FLOAT    Imaginary part of the open loop gain at the
                         calibration line frequency.
-k      FLOAT    Real part of the digital filter at the
                         calibration line frequency.
-l      FLOAT    Imaginary part of digital filter at the
                         calibration line frequency.
-F      STRING   Name of frame cache file.
-S      STRING   Name of segment list file.
-A      STRING   AS_Q channel name (eg, L1:LSC-AS_Q).
-E      STRING   Excitation channel name (eg, L1:LSC-ETMX_EXC_DAQ)
-D      STRING   Darm channel name (eg, L1:LSC-DARM_CTRL)
-b      STRING   Output file for calibration factors.
```

We used the output files produced by Xavier Siemens for the times requested, and re-calculated the α, β coefficients using values g_0, d_0 shown in Table 6. We also show in the same table the

IFO	f_{cal}	g_0	e_g (mag, phase)	d_0	e_d (mag,phase)
L1	927.7 Hz	$0.06372 + i\,0.2299$	1%, 0.5deg	-1.2107 -i 4.9949	0.2%, 0.01deg
H1	973.3 Hz	$0.1667 + i\,0.2240$	0.002%, deg	1.3419 + i 1.8202	0.2%, 0.001deg
H2	973.8 Hz	$0.07682 + i\,0.1753$	0.4%, 0.06deg	2.3159 +i 4.7527	1%, 0.01 deg

Table 6: Calibration frequencies, and magnitude and phase of the open loop gain function $G(f)$ and the digital function $D(f)$ evaluated at the calibration frequencies.

Figure 10: The left column shows the distribution of magnitude and phase angles of the coefficients β and $\alpha\beta$ during the reference time for L1; the figures on the right shows the phase angles of the coefficients during all of S3.

estimates for the errors in g_0, d_0 estimated in magnitude from the means of the real part of $\alpha\beta, \beta$ during the reference time; and in phase, from the mean of the imaginary parts of $\alpha\beta, \beta$ for all of S3.

We show the data used in each case in Figs. 10,11,12. We can see that even if the mean of the phase angle of $\alpha\beta$ is slightly different from zero for H1 and H2, the distribution of the measured values for all of S3 has a Gaussian distribution, as expected. However, the distribution for L1 does not show such a distribution, and suggests a superposition of several distributions with different means, which differ by about a degree. A time series of the imaginary part of $\alpha\beta$ shows that there are not distinct "epochs", but rather a slowly drifting mean with time scales of days. We do not have an explanation for this behavior, other than some element in $A(f)$ or $C(f)$ was changing its frequency dependence during S3 (or at least, its phase at the calibration frequency, 927.7 Hz). In other words, this was probably a real (but not critical) problem with the L1 detector, which was accurately reflected in the measurement. Since this effect only indicates a systematic error of 0.7 degrees in phase for G_0 at 927.7 Hz, and an error 1.4% in the calculated magnitude of $\alpha\beta$, we include this in the appropriate error budget, but otherwise believe the calibration procedure is correct, even in the presence of this unexplained measurement.

We show in Figs 13, 15 and 17 the time series of the calibration coefficients during science times in S3; and in Figs 14 and 16, 18, the distribution of their real and imaginary parts also during S3. The coefficients were calculated every 60 seconds (i.e., using 60 sec as the integration time for each coefficient). From the mean of the distribution of the imaginary parts, we estimate the
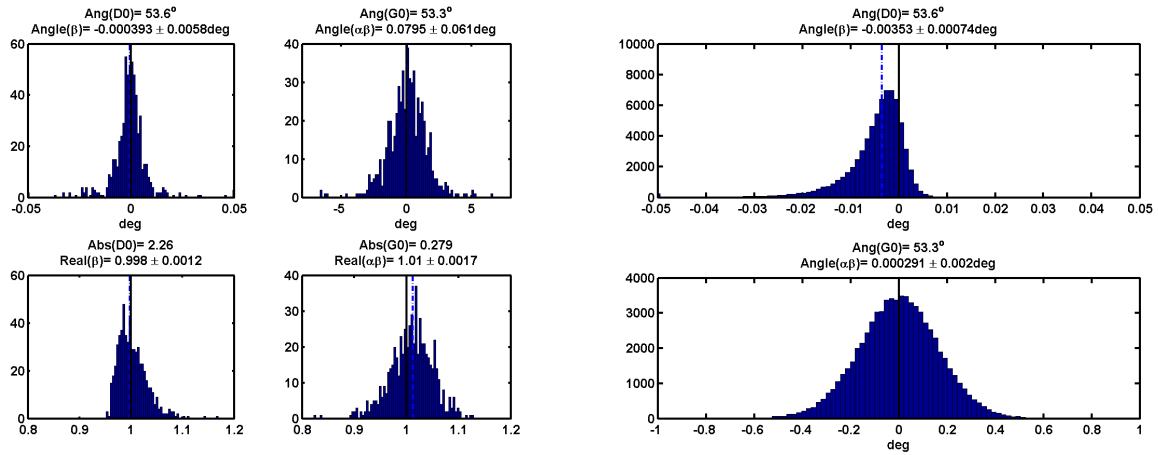
Figure 11: The left column shows the distribution of magnitude and phase angles of the coefficients β and αβ during the reference time for H1; the figures on the right shows the phase angles of the coefficients during all of S3.
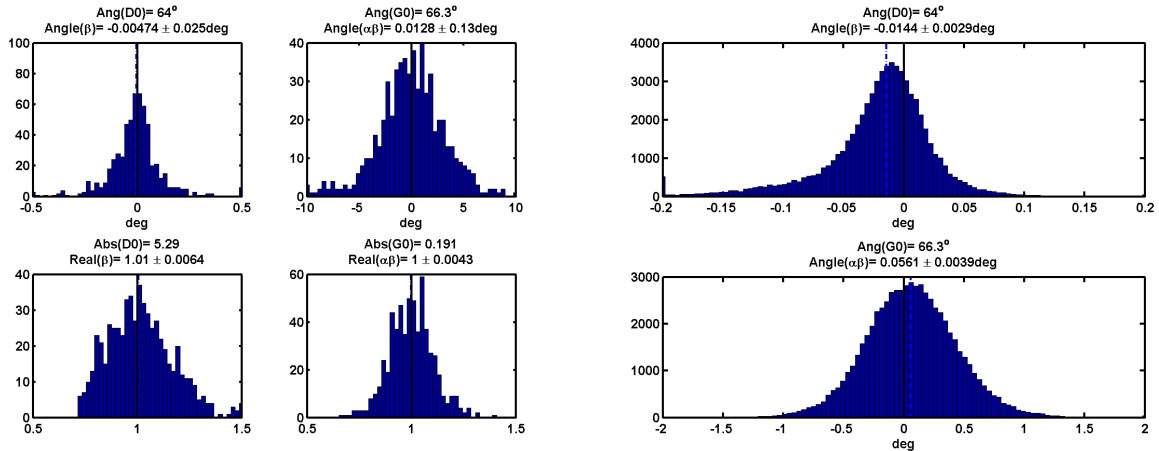

Figure 12: The left column shows the distribution of magnitude and phase angles of the coefficients β and αβ during the reference time for H2; the right column shows the phase angles of the coefficients during all of S3.

systematic error in the corresponding coefficient; from the width of the distribution, we estimate the random error; these are shown in Table 7. We also show in Table 7 the "spread" of the values of the coefficients during the run, which is only an error if a fixed coefficient is used for the whole run. The spread in $\alpha\beta$ is significantly smaller than in α, as expected from the successful implementation of the algorithm calculating the input matrix coefficient (the β coefficient).

IFO	α		β		$\alpha\beta$	
	error	spread	error	spread	error	spread
L1	(1.4%, 0.5%)=1.5%	14%	(0,0.01%)=0.01%	13%	(1.4%, 0.5%)=1.5%	4%
H1	(0, 0.3%)= 0.3%	3%	(0,0.007%)=0.007%	3.5%	(0,0.3%)=0.3%	1.3%
H2	(0,0.6%)=0.6%	2.7%	(0,0.06%)=0.06%	6.2%	(0,0.6%)=0.6%	1.9%

Table 7: Estimated errors for the point estimates of the calibration coefficients (averaged over a minute), and spread of the calibration coefficients over the S3 run.
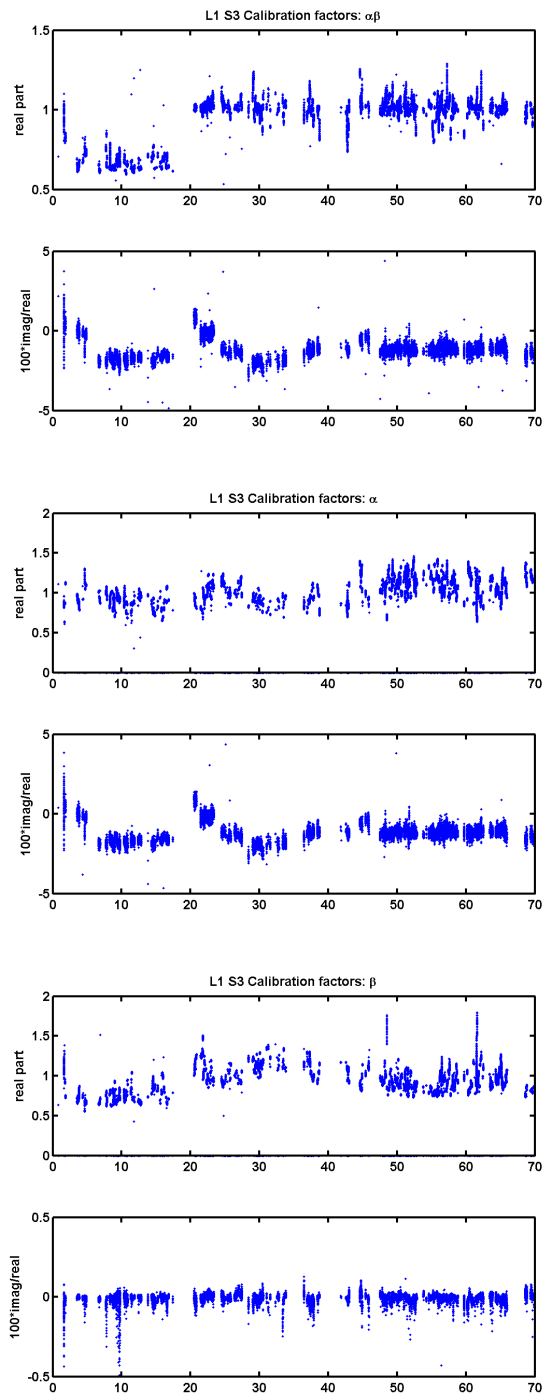
Figure 13: Time series of L1 calibration coefficients during S3. The horizontal axis is in days into S3. Notice the "drift" in the imaginary part of the α coefficient during the first half of the run. Around day 20, after a power outage, the unity gain frequency of the DARM loop was changed, as indicated in the step in the $\alpha\beta$ coefficient.
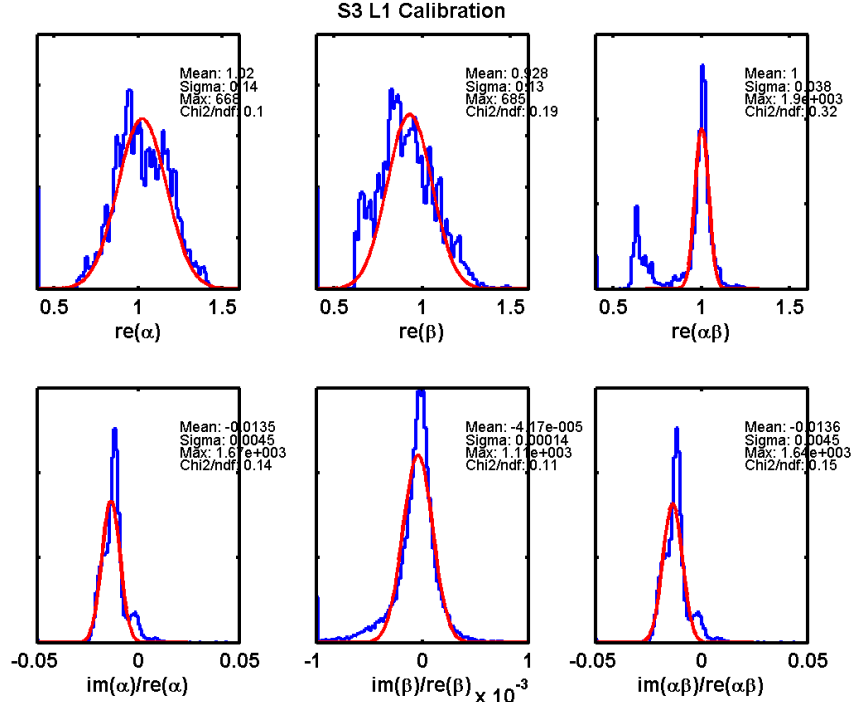
Figure 14: Histogram of real and imaginary parts of L1 calibration coefficients during S3.

6 Response function

The response function at a time t, as a function of frequency f, is given by Eq. 3, which we repeat here again in terms of functions and parameters directly measured:

$$R(t, f) = \frac{1 + \alpha(t)\beta(t)G_0(f)}{\alpha(t)C_0(f)} = A(f)D_0(f)\frac{1 + \alpha(t)\beta(t)G_0(f)}{\alpha(t)G_0(f)}.$$

We post in the calibration web page a frequency series (in text and frame format) for the response function at the reference time (when the open loop gain is measured, and we assume $\alpha = \beta = 1$). The plots for the reference response functions are shown in Fig19.

6.1 Response functions: errors

If we define $R' = R + \Delta R$ as a calculated response function different from the true response function R, we define the error in magnitude and phase as

$$\frac{\Delta |R|}{|R|} = \frac{|R'| - |R|}{|R|} \approx \Re\frac{\Delta R}{R} \tag{5}$$

$$\Delta\Phi_R = \frac{R'/|R'|}{R/|R|} - 1 \approx \Im\frac{\Delta R}{R} \tag{6}$$

We estimate errors in the response function assuming independent errors in $A(f)$, $D_0(f)$, $G_0(f)$, $\alpha(t)$ and $\beta(t)$. We see, for example, that relative errors in magnitude or phase for the
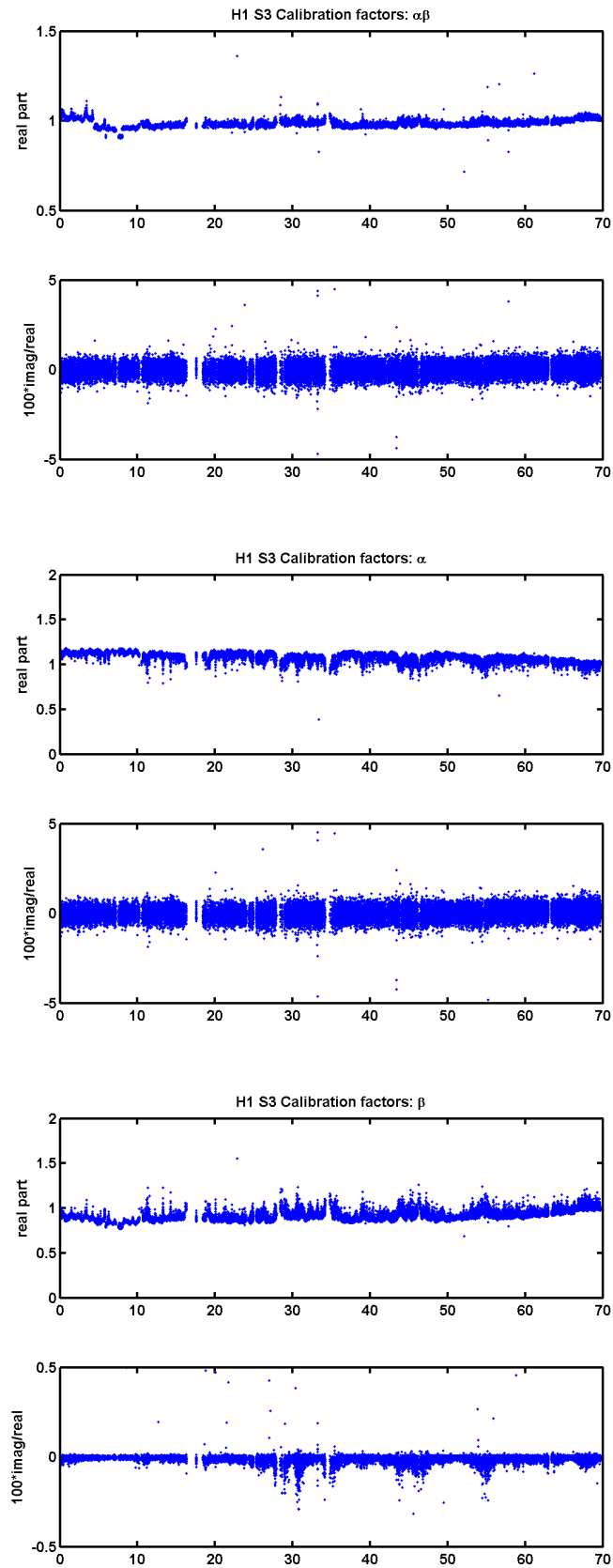
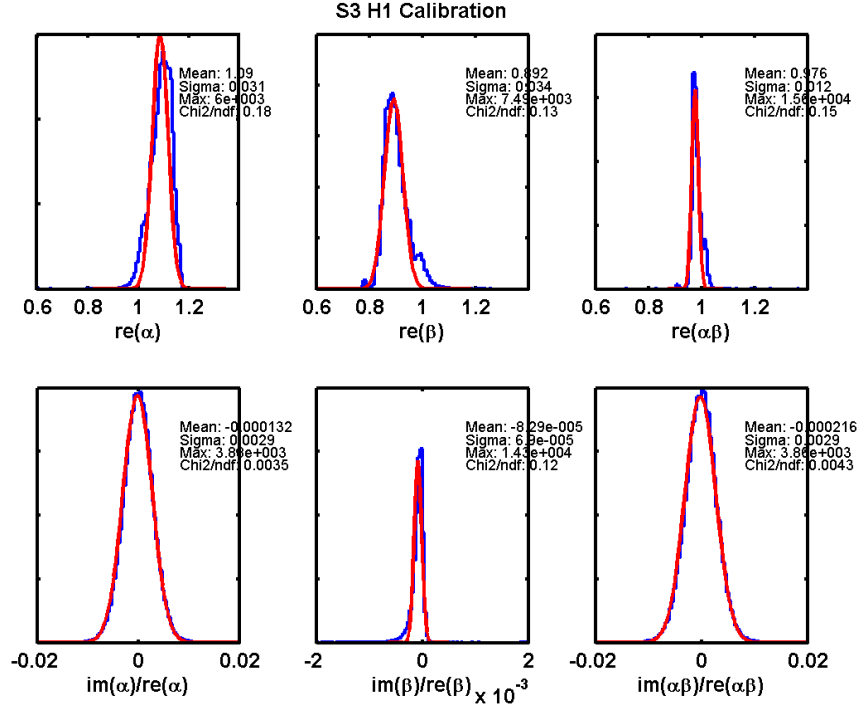Figure 15: Time series of H1 calibration coefficients during S3. The horizontal axis is in days into S3.

Figure 16: Histogram of real and imaginary parts of H1 calibration coefficients during S3.

actuation function $A(f)$ or in the digital filter function $D(f)$ will introduce the same relative errors in the response function, and the errors will be independent of time.

In order to estimate the errors defined in Eq.5,6, we take logarithmic partial derivatives of $\Delta|R|$ and partial derivatives of $\Delta\phi_R$ with respect to magnitude and phase of $A(f)$, $G(f)$, $D(f)$, and with respect to α and β, and then add the errors in each parameter in quadrature, using the square of the partial derivatives as weighting functions. We evaluate the partial derivatives at the reference time, when $\alpha = \beta = 1$.

We begin by calculating the complex function $\Delta R/R$:

$$
\begin{aligned}
\frac{\Delta R}{R} &= \frac{\Delta A}{A} + \frac{\Delta D_0}{D_0} + \frac{1}{1 + \alpha\beta G_0}\frac{\Delta G_0}{G_0} + \frac{1}{1 + \alpha\beta G_0}\frac{\Delta\alpha}{\alpha} + \frac{\alpha\beta G_0}{1 + \alpha\beta G_0}\frac{\Delta\beta}{\beta} \\
&= \frac{\Delta A}{A} + \frac{\Delta D_0}{D_0} + \frac{1}{1 + G_0}\frac{\Delta G_0}{G_0} + \frac{1}{1 + G_0}\frac{\Delta\alpha}{\alpha} + \frac{G_0}{1 + G_0}\frac{\Delta\beta}{\beta}
\end{aligned}
$$

Next, we get a formula for $\Delta|R|/|R|$ and $\Delta\phi_R$ from the real and imaginary part of $\Delta R/R$:
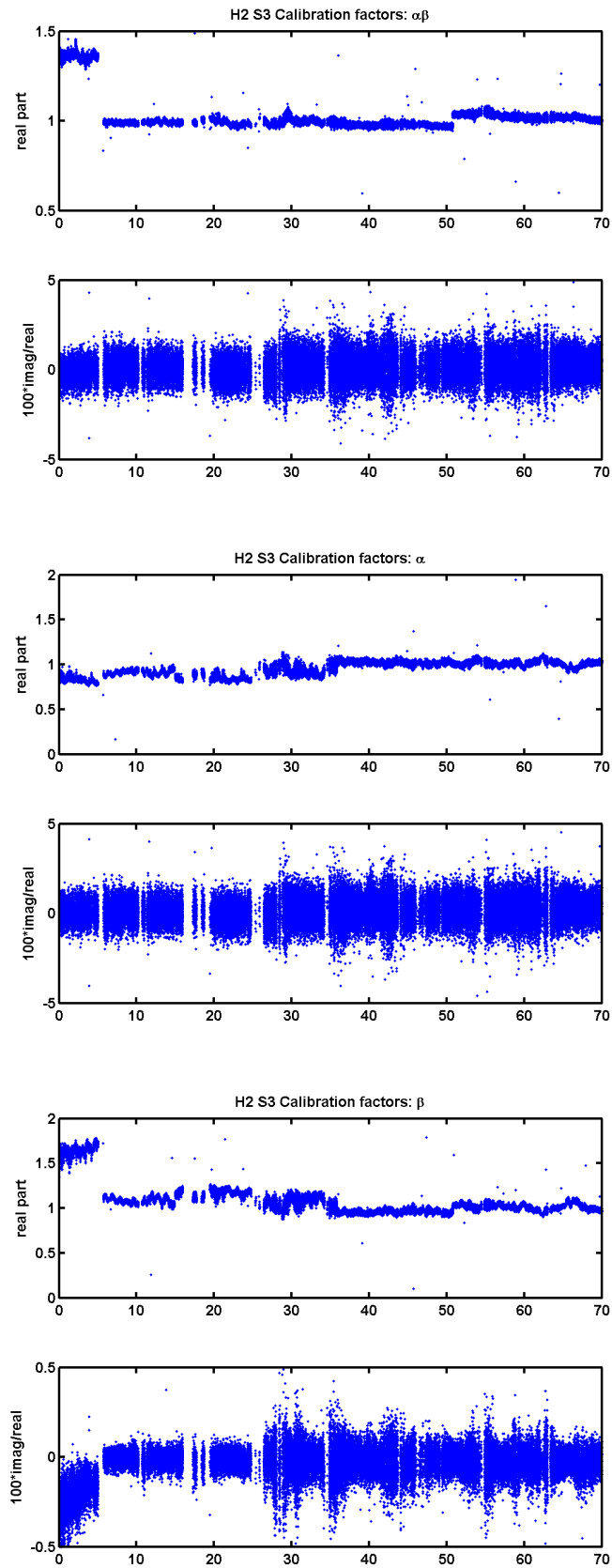
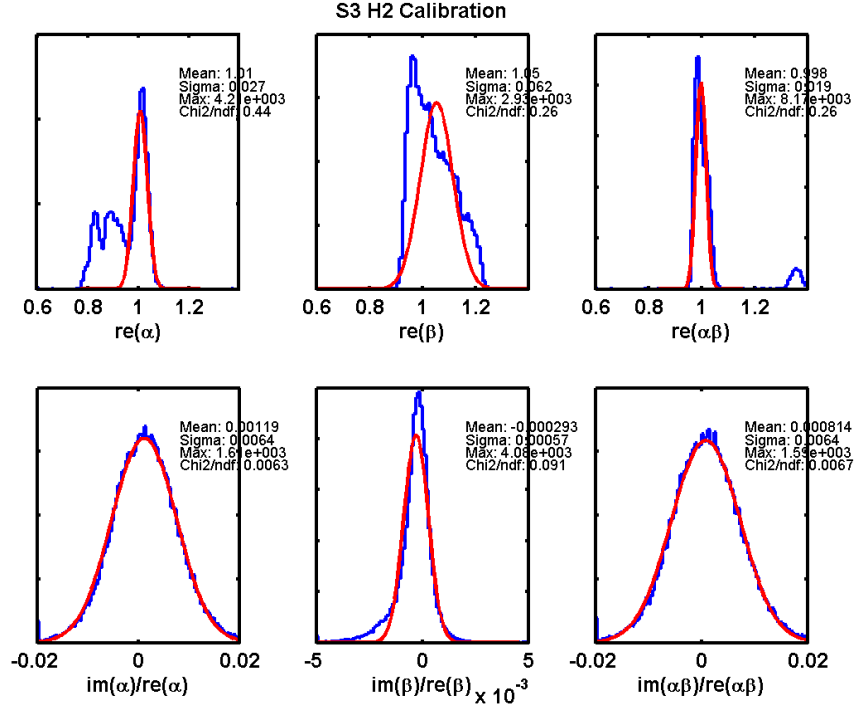Figure 17: Time series of H2 calibration coefficients during S3. The horizontal axis is in days into S3.

Figure 18: Histogram of real and imaginary parts of H2 calibration coefficients during S3.

$$
\begin{aligned}
\frac{\Delta|R|}{|R|} &= \Re\left(\frac{\Delta R}{R}\right) \\
&= \Re\frac{\Delta A}{A} + \Re\frac{\Delta D_0}{D_0} + \Re\frac{1}{1+G_0}\frac{\Delta G_0}{G_0} + \Re\frac{1}{1+G_0}\frac{\Delta\alpha}{\alpha} + \Re\frac{G_0}{1+G_0}\frac{\Delta\beta}{\beta} \\
&= \frac{\Delta|A|}{|A|} + \frac{\Delta|D_0|}{|D_0|} + \left(\Re\frac{1}{1+G_0}\right)\Re\left(\frac{\Delta G_0}{G_0}\right) - \left(\Im\frac{1}{1+G_0}\right)\Im\left(\frac{\Delta G_0}{G_0}\right) \\
&\quad + \Re\left(\frac{1}{1+G_0}\right)\frac{\Delta\alpha}{\alpha} + \Re\left(\frac{G_0}{1+G_0}\right)\frac{\Delta\beta}{\beta} \\
&= \frac{\Delta|A|}{|A|} + \frac{\Delta|D_0|}{|D_0|} + \frac{\Re(1+G_0)}{|1+G_0|^2}\frac{\Delta|G_0|}{|G_0|} + \frac{\Im G_0}{|1+G_0|^2}\Delta\phi_{G_0} \\
&\quad + \frac{\Re(1+G_0)}{|1+G_0|^2}\frac{\Delta\alpha}{\alpha} + \Re\left(\frac{G_0}{1+G_0}\right)\frac{\Delta\beta}{\beta} \\
&= \frac{\Delta|A|}{|A|} + \frac{\Delta|D_0|}{|D_0|} + C_R\frac{\Delta|G_0|}{|G_0|} + C_I\Delta\phi_{G_0} + C_R\frac{\Delta\alpha}{\alpha} + C_{R\beta}\frac{\Delta\beta}{\beta}
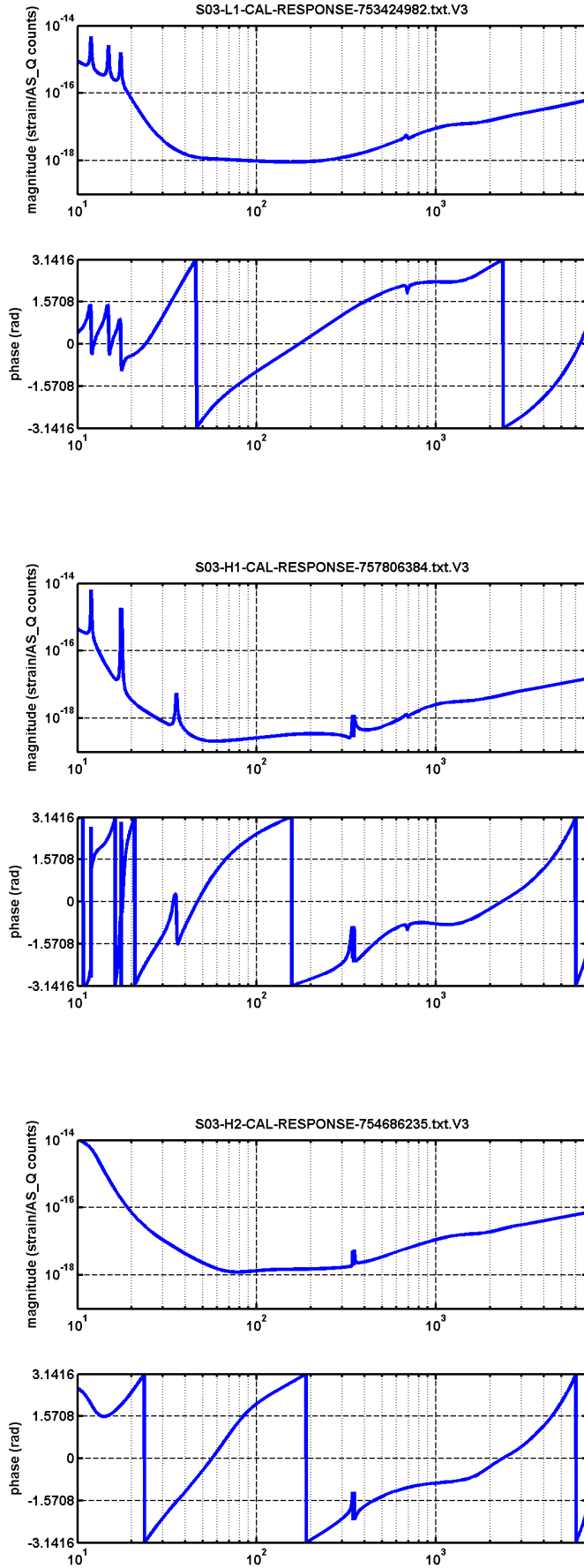\end{aligned}
\tag{7}
$$

S03-L1-CAL-RESPONSE-753424982.txt.V3

S03-H1-CAL-RESPONSE-757806384.txt.V3

S03-H2-CAL-RESPONSE-754686235.txt.V3

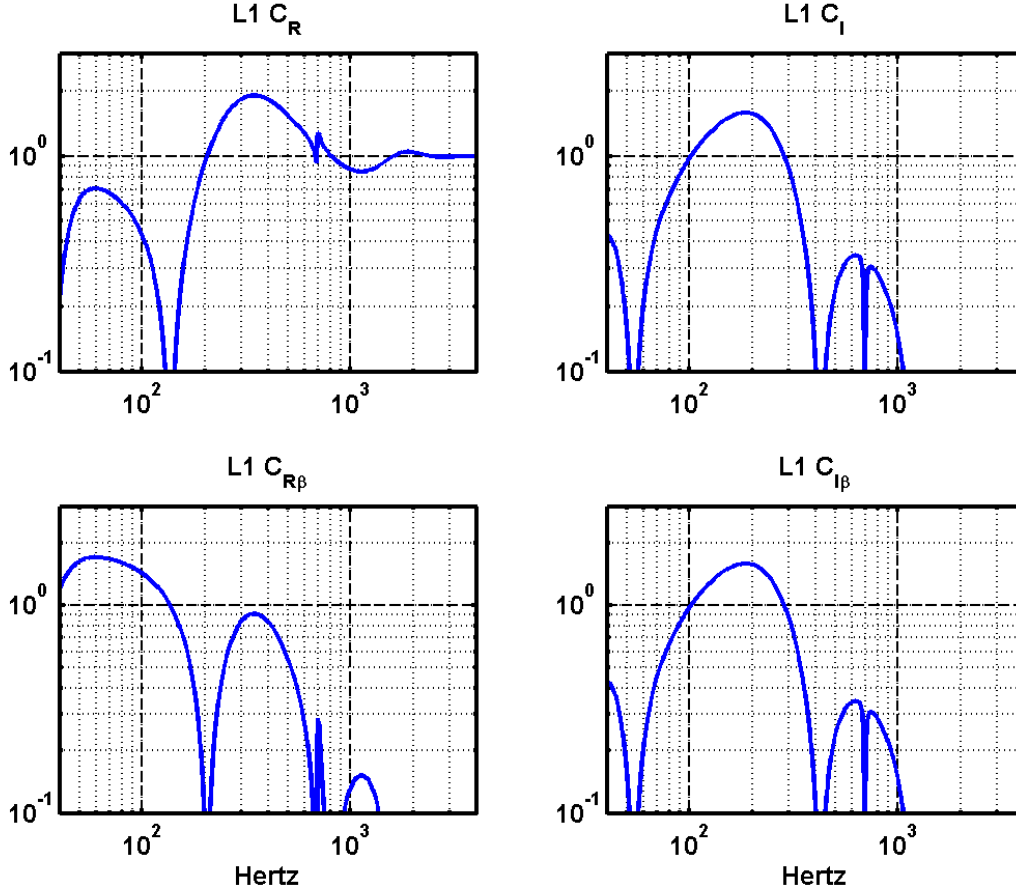Figure 19: Reference response functions for the LIGO detectors during S3.

Figure 20: Coefficients C_R, C_I, $C_{R\beta}$, $C_{I\beta}$ calculated with L1 open loop gain function.

$$
\begin{aligned}
\Delta\phi_R &= \Im\left(\frac{\Delta R}{R}\right) \\
&= \Im\frac{\Delta A}{A} + \Im\frac{\Delta D_0}{D_0} + \Im\frac{1}{1+G_0}\frac{\Delta G_0}{G_0} + \Im\frac{1}{1+G_0}\frac{\Delta\alpha}{\alpha} + \Im\frac{G_0}{1+G_0}\frac{\Delta\beta}{\beta} \\
&= \Delta\phi_A + \Delta\phi_D + \left(\Re\frac{1}{1+G_0}\right)\Im\left(\frac{\Delta G_0}{G_0}\right) + \left(\Im\frac{1}{1+G_0}\right)\Re\left(\frac{\Delta G_0}{G_0}\right) \\
&\quad + \Im\left(\frac{1}{1+G_0}\right)\frac{\Delta\alpha}{\alpha} + \Im\left(\frac{G_0}{1+G_0}\right)\frac{\Delta\beta}{\beta} \\
&= \Delta\phi_A + \Delta\phi_D + C_R\Delta\phi_G + C_I\frac{\Delta|G_0|}{|G_0|} + C_I\frac{\Delta\alpha}{\alpha} + C_{I\beta}\frac{\Delta\beta}{\beta}
\end{aligned}
\tag{8}
$$

We have defined weighting functions to simplify the formulas[1]:

$$C_R = \Re\left(\frac{1}{1+G_0}\right)$$

$$C_I = \Im\left(\frac{1}{1+G_0}\right) \tag{9}$$

$$C_{R\beta} = \Re\left(\frac{G_0}{1+G_0}\right)$$

$$C_{I\beta} = \Im\left(\frac{G_0}{1+G_0}\right) \tag{10}$$

From Eq. 7,8 we can now easily calculate partial derivatives, and obtain formulas for the error in the magnitude and phase of the response function:

$$\left(\frac{\Delta|R|}{|R|}\right)^2 = \left(\frac{\Delta|A|}{|A|}\right)^2 + \left(\frac{\Delta|D_0|}{|D_0|}\right)^2 + C_R^2\left(\frac{\Delta|G_0|}{|G_0|}\right)^2 + C_I^2\left(\Delta\phi_{G_0}\right)^2 + C_R^2\left(\frac{\Delta\alpha}{\alpha}\right)^2 + C_{R\beta}^2\left(\frac{\Delta\beta}{\beta}\right)^2 \tag{11}$$

$$\left(\Delta\phi_R\right)^2 = \left(\Delta\phi_A\right)^2 + \left(\Delta\phi_D\right)^2 + C_R^2\left(\Delta\phi_G\right)^2 + C_I^2\left(\frac{\Delta|G_0|}{|G_0|}\right)^2 + C_I^2\left(\frac{\Delta\alpha}{\alpha}\right)^2 + C_{I\beta}^2\left(\frac{\Delta\beta}{\beta}\right)^2 \tag{12}$$

The coefficients C_R and C_I are plotted in Figure 20 using values from L1. Obviously they enhance or reduce the effect of some contributions depending on the frequency.

We use the formulas 11,12 with the errors estimated in previous sections to calculate the total errors in the magnitude and phase of the response function. The parameters used in this calculation are summarized in Table 8. The individual contributions, and the total error between 40 Hz and 2kHz is shown in Figs21,22,23. A summary table of errors in magnitude and phase is shown in Table 9.

Error	L1	H1	H2
$\Delta|A|/|A|$	0.15	0.08	0.02
$\Delta\phi_A$	1.5deg	1.5deg	0.75 deg
$\Delta|D|/|D|$	0.02	0.02	0.02
$\Delta\phi_D$	0	0	0
$\Delta|G|/|G|$	0.05	0.04	0.10
$\Delta\phi_G$	1deg	2deg	2deg
$\Delta\alpha/\alpha$	0.015	0.003	0.006
$\Delta\beta/\beta$	10^{-4}	0.7×10^{-4}	6×10^{-4}

Table 8: Errors used to calculate the total error in response function.

---

[1]There is a typo in formulas (9) and (10) used in [2] T040060-01 to define coefficients C_R and C_I. The coefficients defined there are the squares of the coefficients defined here in 9.
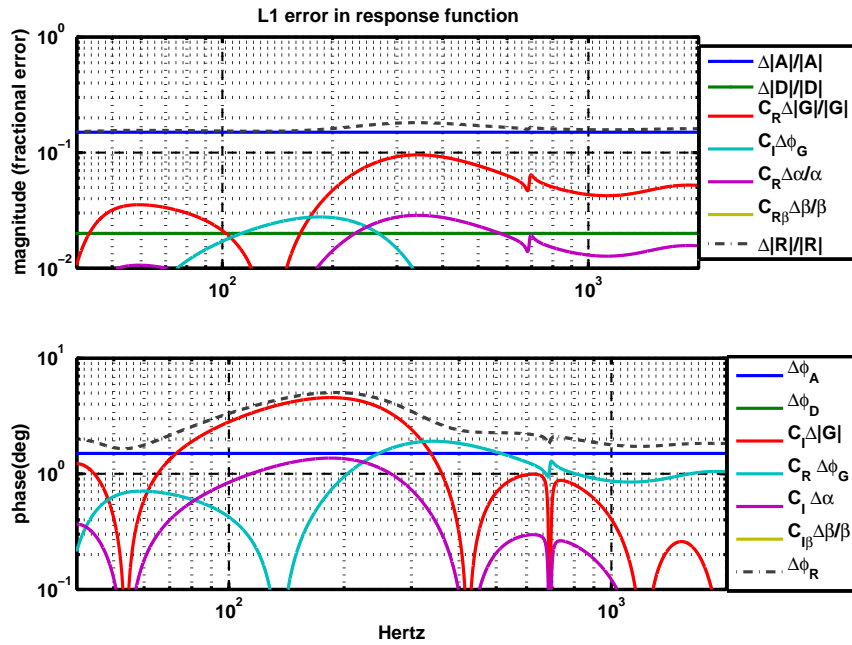
Figure 21: Error in magnitude and phase of L1 response function. The error contributions in the legend, but not visible in the plot are smaller than 1% in magnitude, 0.1 deg in phase.
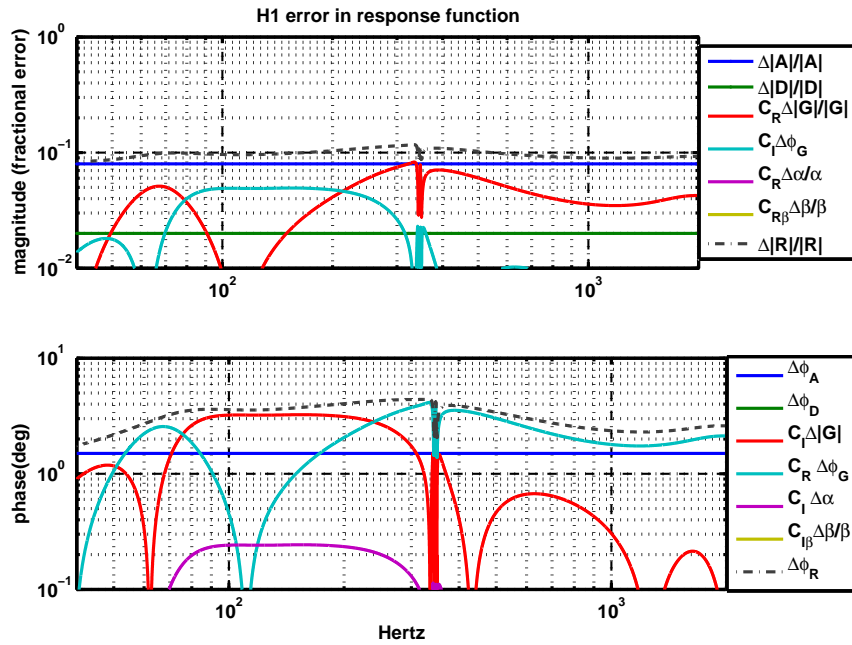
Figure 22: Error in magnitude and phase of H1 response function. The error contributions in the legend, but not visible in the plot are smaller than 1% in magnitude, 0.1 deg in phase.
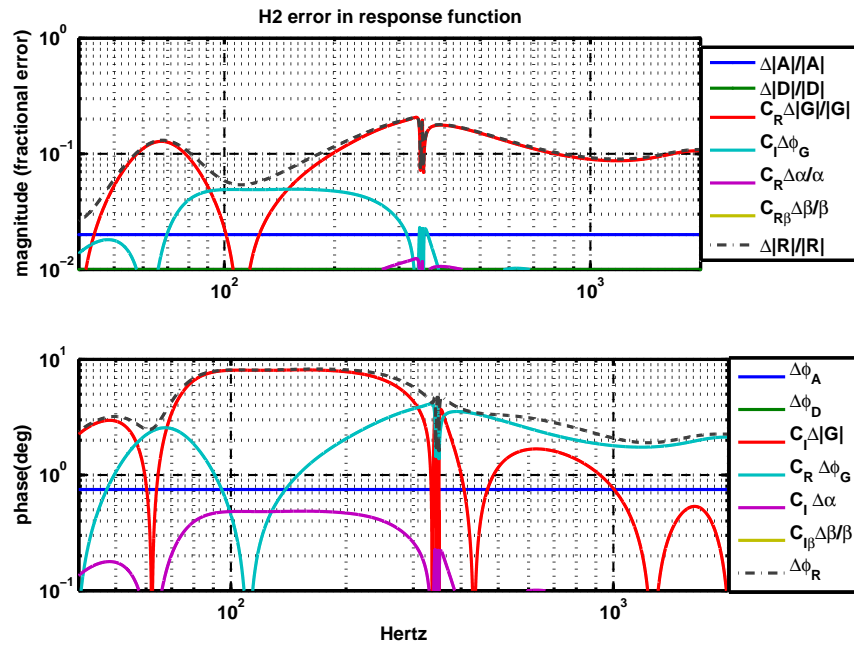
Figure 23: Error in magnitude and phase of H2 response function. The error contributions in the legend, but not visible in the plot are smaller than 1% in magnitude, 0.1 deg in phase; except for $\Delta|A|/|A|$ which is 2% and hides behind $\Delta|D|/|D|$, which is also 2%.

IFO	$\Delta|R|/|R|$	$\Delta\phi_R$	min $\Delta|R|/|R|$	min $\Delta\phi_R$	max $\Delta|R|/|R|$	max $\Delta\phi_R$
L1	15.4%	3.3deg	15.3%	1.7deg	18.1%	5.0 deg
	@ 100 Hz		@127 Hz	@1182 Hz	@339 Hz	@190 Hz
H1	9.6%	3.6deg	8.7%	2.1deg	11.7%	4.4 deg
	@ 100 Hz		@350 Hz	@350 Hz	@334 Hz	@332 Hz
H2	5.8%	8.1deg	5.4%	1.6deg	20.9%	8.3 deg
	@ 100 Hz		@111 Hz	@350 Hz	@335 Hz	@166 Hz

Table 9: Errors in magnitude and phase of response functions for the three interferometers, at 100Hz. Also shown are the maxima and minima in error in the range 60Hz-2kHz.

7 Conclusions

We have presented the methods used to obtain the final calibration of the LIGO detectors during the third Science Run, and estimated errors associated with the calibration.

The calibration files and matlab files with the models used to generate the calibration files are posted in the calibration home page, for S3(V3):

```
http://blue.ligo-wa.caltech.edu/engrun/Calib_Home/
```

The main differences from this calibration with respect to previous runs are:

- improved methods to obtain the DC actuation calibration at LHO, especially for H2;

- a time-varying β parameter that reduced the fluctuations in the open loop gain (measured by the product $\alpha\beta$) due to optical gain fluctuations (or α); and

- the measurement of the calibration coefficients using demodulation of the stored data channels, rather than from power spectral estimates.

References

[1] Adhikari R., Fritschel P., González G., Landry M., Matone L., O'Reilly B.,Radkins H., Takamori A. *Calibration of the LIGO detectors for the First LIGO Scientific Run*
`LIGO-T030097-00-D`

[2] G. González, M. Landry, B, O'Reilly, H. Radkins *Calibration of the LIGO detectors for S2*
`LIGO-T040060-01-D`

[3] Adhikari R, Evans M, Landry M, Marka S, Matone L and Yamamoto H *Input test mass (ITM) absolute calibrations: fringe counting, fringe fitting, and sign toggling methods*
`LIGO-T020141-00-D`

[4] See entries on LLO elog n 01/22/2005 for details on the time variation in the input matrix coefficient, and its effects on the gravitational wave channel.